**Max-Planck-Institut
für Mathematik
in den Naturwissenschaften
Leipzig**

A free boundary problem for cell motion

by

Jan Fuhrmann and Angela Stevens

Preprint no.: 32 2013

A free boundary problem for cell motion

Jan Fuhrmann*, Angela Stevens †

March 11, 2013

Abstract

The ability of a large variety of eukaryotic cells to actively move along different substrates plays a vital role in many biological processes. A key player in these processes is the cytoskeleton.

In [7] we introduced a minimal hyperbolic-parabolic model for the reorganization of the actin cytoskeleton of a generic cell resting on a flat substrate and turning into a polarized state upon some external cue. In this paper we derive moving boundary conditions for the same cytoskeleton model and by this allow for the description of actual motion. For the free boundary problem we prove short time well-posedness for a wide class of initial conditions and analyze the emergence of Dirac measures in the densities of actin filament tips. These have a direct biophysical interpretation as sharp polymerization fronts which are experimentally observed in [19], for example.

Further, numerical results will illustrate both, the motion of an initially symmetric resting cell and the emergence of sharp fronts of actin filaments from initially smooth distributions.

1 Introduction

Actin-driven motility is observed and plays a crucial role for eukaryotic cells as different as hunting amebae [10], human fibroblasts controlling wound healing [1], growing axons of neurons in vertebrates' central nervous systems [15], and cancer cells spreading out for metastasis [20]. The mechanism underlying these different types of motion is the constant remodeling of the cytoskeleton which essentially is comprised of actin filaments, myosin motors, and dozens of regulatory and cross-linking proteins. Whereas the latter differ from cell to cell, the polymerization and depolymerization of actin filaments and their displacement by myosin motors are features all these different cell types have in common.

For this reason in [7] we proposed a minimal model for the dynamics of the cytoskeleton which describes the densities of left and right oriented barbed and pointed ends of filaments, and the concentration of actin monomers. Together a system of four hyperbolic conservation laws for the filament tips and a reaction diffusion equation for the monomers on a fixed spatial domain resulted.

*Ruprecht-Karls-Universtität Heidelberg, Institute of Applied Mathematics, Im Neuenheimer Feld 294, D-69120 Heidelberg, jan.fuhrmann@uni-hd.de

†Westfälische Wilhelms-Universtität Münster, Applied Mathematics Münster, Einsteinstraße 62, D-48149 Münster, angela.stevens@wwu.de

In [7] the polarization of the initially symmetric cytoskeleton upon some external stimulus leading to an asymmetry in the coefficient functions which describes the polymerization dynamics of actin monomers at the different types of filament tips was investigated. Here, we formulate moving boundary conditions for this hyperbolic-parabolic model. This allows the cell membrane to be actually displaced and motion to be initiated.

Moreover, the free boundary is compatible with the hyperbolic structure of the equations for the filament tips and we thus can show local in time well posedness for a much wider class of initial conditions than before. This is achieved by a contraction mapping argument. The required estimates rely on the particular shape of the coupling between the hyperbolic equations and the boundary conditions on the one hand and the parabolic equation on the other hand.

Rather than proving global existence of smooth solutions we can explicitely construct measure valued solutions for the end densities. These Dirac measures can be interpreted as sharp fronts of polymerizing actin filaments which are observed in live cell experiments as in [19].

It is very hard to show the emergence of such concentrated measures from smooth data analytically but numerical results provide good evidence for this phenomenon. Our simulations also show examples of cells which are driven into directed motion from an initially symmetric resting state.

2 Derivation of the free boundary problem

We first recall the model in [7] for the kinetics of the cytoskeleton of a cell on a flat substrate which may receive a cue to move into a particular direction – say to the right. Let B denote the density of fast growing (barbed) filament ends and P that of slowly growing (pointed) ones. Then

$$\begin{aligned}
\partial_t B_r &= -\partial_x \left(v_B(a) B_r\right) \equiv \partial_x \left((v_R - \delta\, \kappa_B (a - a_B)) B_r\right) && \text{(2.1a)}\\
\partial_t B_l &= \partial_x \left(v_B(a) B_l\right) && \text{(2.1b)}\\
\partial_t P_r &= -\partial_x \left(v_P(a) P_r\right) \equiv \partial_x \left((v_R + \delta\, \kappa_P (a - a_P)) P_r\right) && \text{(2.1c)}\\
\partial_t P_l &= \partial_x \left(v_P(a) P_l\right) && \text{(2.1d)}
\end{aligned}$$

where the subscripts r and l denote the tips of filaments whose barbed ends are pointing to the right and left, respectively. Here, v_R denotes the myosin-driven retrograde flow velocity, $\kappa_{B/P}$ are the polymerization rate constants and $a_{B/P}$ the critical monomer concentrations for polymerization at barbed and pointed ends, respectively, accounting for the polymerization speed of these ends.

For the monomer concentration a we have

$$\partial_t a - D \partial_{xx} a + \delta\, \kappa_B (a - a_B)(B_r + B_l) + \delta\, \kappa_P (a - a_P)(P_r + P_l) = 0.$$

The linear reaction terms seem at first glance oversimplified since for actin dynamics at barbed ends two regimes are reported with significantly larger κ_B in case the actual actin concentration lies below a_B (see figure 2b in [2]). This is however not problematic as we will see that the monomer concentration does not drop below the critical concentration a_B whenever it initially lies above this value.

In order to write the system in a more concise form we define

$$\begin{aligned} u &= (u^1,\, u^2,\, u^3,\, u^4)^T := (B_l,\, P_r,\, P_l,\, B_r)^T, \\ \Lambda &= \operatorname{diag}(\lambda^1,\, \lambda^2,\, \lambda^3,\, \lambda^4) := \operatorname{diag}(-v_B,\, v_P, -v_P,\, v_B). \end{aligned}$$

Using these notations we can reduce the equations to

$$\partial_t u + \partial_x(\Lambda u) = 0 \tag{2.2}$$

$$\partial_t a - D\partial_{xx} a = R(a,u) \equiv -c\cdot u\, a + \tilde{c}\cdot u, \quad \text{where} \tag{2.3}$$

$$c = \delta(\kappa_B,\, \kappa_P,\, \kappa_P,\, \kappa_B) \quad \text{and} \quad \tilde{c} = \delta(\kappa_B a_B,\, \kappa_P a_P,\, \kappa_P a_P,\, \kappa_B a_B)$$

The most basic interaction between the filament ends and the boundary is an infinitely soft membrane that exerts no forces on the filaments and is therefore supported by the outermost tips that move at their free velocity λ^α ($\alpha = 1, \ldots, 4$). Since the hyperbolic part is diagonal we can directly read off the characteristic velocities of the respective end densities and write for the left and right boundary curves

$$l(t) = \min_{\alpha=1,\ldots,4} l^\alpha(t) \qquad \text{and} \qquad r(t) = \max_{\alpha=1,\ldots,4} r^\alpha(t), \tag{2.4}$$

respectively. Here, for $\alpha = 1, \ldots, 4$ the boundary curves of the α^{th} characteristic family are given by the initial value problems

$$\begin{aligned} \dot{l^\alpha}(t) &= \lambda^\alpha(a(t, l^\alpha(t))), & l^\alpha(0) &:= l_0^\alpha \equiv \min \operatorname{supp} u_0^\alpha \\ \dot{r^\alpha}(t) &= \lambda^\alpha(a(t, r^\alpha(t))), & r^\alpha(0) &:= r_0^\alpha \equiv \max \operatorname{supp} u_0^\alpha \end{aligned}$$

with initial values given by the outer points of the support of the initial data u_0^α of the respective end density.

For the characteristic families which are not the leading ones we prescribe zero boundary conditions since no filaments enter the cell from outside. For the leading characteristic families which are the end densities supporting the membrane, we have a characteristic boundary and therefore the boundary values are given by the evolution of the respective equation itself.

On the resulting space-time domain

$$Q_T = \left\{(t,x) \in \mathbb{R}^2 \mid 0 < t < T, l(t) < x < r(t)\right\} \tag{2.5}$$

we impose no-flux conditions for the actin monomers which are assumed to be reflected at the membrane. We therefore have

$$\begin{aligned} D\partial_x a(t,l(t)) + a(t,l(t))\,\dot{l}(t) &= 0 \quad \text{for } 0 < t < T \\ D\partial_x a(t,r(t)) + a(t,r(t))\,\dot{r}(t) &= 0 \quad \text{for } 0 < t < T. \end{aligned} \tag{2.6}$$

Let the initial data satisfy

$$u(0,x) = u_0(x) \geq 0, \quad a(0,x) = a_0(x) \geq 0 \qquad \text{for } x \in [0, L] \tag{2.7}$$

For obvious physical reasons we also assume the initial end densities to be such that the barbed ends of the right oriented filaments are located further to the right than the corresponding pointed ends,

$$\int_0^x u_0^2(y)\mathrm{d}y > \int_0^x u_0^4(y)\mathrm{d}y \qquad \text{for each } x \in (0, L),$$

and likewise for the left oriented filaments. Since we do not consider filament branching here, the total amount of barbed ends of either orientation equals the total amount of corresponding pointed ends.

Moreover, we assume $a_B \leq a_0 \leq a_P$. This bound will be shown to be preserved for any sufficiently smooth solution of the free boundary problem.

3 Short time well posedness

In this section we show the existence of a unique solution to the problem (2.2), (2.3), (2.4), (2.6), (2.7), denoted by (FBP), for small times T.

First, we derive some general bounds being necessarily satisfied by any sufficiently smooth solution of the problem. Physical considerations lead us to the following conditions on the model parameters which shall be assumed to be satisfied throughout the text.

Condition 3.1. *(i)* v_R *and* δ *are positive constants*

(ii) $\kappa_B,\ \kappa_P,\ a_B,$ *and* a_P *belong to* $C^{0,1}([0,T];\ C^\infty(\mathbb{R}))$ *and satisfy*

$$\inf_{t,x} a_B(t,x) =: \underline{a_B} > 0 \qquad \textit{and} \qquad \sup_{t,x} a_P(t,x) =: \overline{a_P} < \infty.$$

(iii) At barbed ends, the affinity for monomers is higher and the reaction kinetics are faster than at pointed ends:

$$\begin{aligned} \sup_{t,x} a_B(t,x) =: \overline{a_B} \quad &< \quad \underline{a_P} := \inf_{t,x} a_P(t,x) \\ \sup_{t,x} \kappa_P(t,x) \quad &< \quad \inf_{t,x} \kappa_B(t,x). \end{aligned}$$

(iv) To allow for positive values of v_B *we assume*

$$\sup_{t,x} \left(\kappa_B(t,x)(a_P(t,x) - a_B(t,x))\right) \ > \ \frac{v_R}{\delta}.$$

Now we can define what we mean by a physical solution for problem (FBP).

Definition 3.1. *A* smooth solution *of problem* (FBP) *is a pair*

$$(u,\, a) \in C_b^1\left(\overline{Q_T};\, [0,\infty)^n\right) \times \left(C_b^{2_x,1_t}(Q_T;\, (0,\infty)) \cap C^{1_x,0_t}(\overline{Q_T};\, (0,\infty))\right)$$

such that u *satisfies* (FBP) *on* Q_T *given by 2.5.*

Such a solution is called a physical smooth solution *if the end densities in addition satisfy*

$$\alpha_l(t) \cap \{1,2\} \neq \emptyset, \qquad \alpha_r(t) \cap \{3,4\} \neq \emptyset \qquad \text{for each } t \in [0,T] \tag{3.1}$$

where $\alpha_{l/r}(t)$ *denote the leading characteristic families, i.e.* $\alpha \in \alpha_l(t)$ *if*

$$l^\alpha(t) \leq l^{\alpha'}(t) \qquad \textit{for all } \alpha' \in \{1,\dots,4\}\backslash\{\alpha\}$$

and in case of equality for some α' *in addition* $\lambda^\alpha(t,l(t)) \leq \lambda^{\alpha'}(t,l(t))$ *holds. The leading characteristic families on the right boundary curve are defined similarly.*

In the following we will only deal with such physical solutions since the membrane on the left can only be supported by pointed ends of right oriented filaments or by barbed ends of left oriented ones, and similarly for the right boundary.

The first observation is that for any $u \in [0,\infty)^4$:

$$\begin{aligned} R(a_P(t,x),u) &= -\delta\,\kappa_B(t,x)(a_P(t,x)-a_B(t,x))(u^1+u^4) \le 0 \\ R(a_B(t,x),u) &= \delta\,\kappa_P(t,x)(a_P(t,x)-a_B(t,x))(u^2+u^3) \ge 0. \end{aligned}$$

These inequalities are strict whenever one of the involved end densities is positive. As a consequence we obtain the following bound on a.

Lemma 3.1. *Assume, the parameters satisfy*

$$\frac{v_R}{\delta} < \min\left\{ \inf_{t,x} \kappa_B(t,x)(\overline{a_P}-\overline{a_B}),\ \inf_{t,x} \kappa_P(t,x)(\underline{a_P}-\underline{a_B}) \right\}. \tag{3.2}$$

Then, any smooth physical solution of (FBP) with

$$\underline{a_B} \le a(0,x) \le \overline{a_P} \qquad \text{for each } x \in [0,L]$$

satisfies

$$\underline{a_B} \le a(t,x) \le \overline{a_P} \qquad \text{for each } (t,x) \in \overline{Q_T}.$$

Proof. If a takes the value $\underline{a_B}$ at some point (t_0,x_0) in the interior of Q_T without having reached it before then it has a local minimum at this point and the signs of both, the diffusion term and the reaction term, yield $\partial_t a(t_0,x_0) \ge 0$, and a cannot decrease anymore. Likewise, a will not grow once it attains the value $\overline{a_P}$ in the interior of the domain.

If the value $\underline{a_B}$ is reached at the left boundary, say at $(t_0,l(t_0))$, then the hypotheses yield strictly positive velocities λ^1 and λ^2 at this point. The boundary conditions then lead to

$$\partial_x a(t_0,l(t_0)) < 0$$

which implies $a < \underline{a_B}$ in some neighborhood lying inside Q_T which contradicts the above. Similarly, a cannot attain $\overline{a_P}$ at the left boundary and neither of $\underline{a_B}$ or $\overline{a_P}$ at the right boundary. □

Corollary 3.2. *Under the hypotheses of Lemma 3.1, the reaction term in (2.3) satisfies*

$$-2\delta \sup_{t,x} \kappa_B(\overline{a_P}-\underline{a_B})\|u\|_{C^0} \le R(a(t,x),u(t,x)) \le 2\delta \sup_{t,x} \kappa_P(\overline{a_P}-\underline{a_B})\|u\|_{C^0}$$

where

$$\|u\|_{C^0} = \sup_{(t,x)\in\overline{Q_T}} \max_{\alpha=1,\dots,4} |u^\alpha(t,x)|.$$

Since

$$\lambda^1(t,x) = v_B(a(t,x)) = \lambda^4(t,x)\ , \quad \lambda^2(t,x) = v_P(a(t,x)) = -\lambda^3(t,x)$$

we immediately deduce from the bound on a that for $\alpha = 1,\dots,4$:

$$|\lambda^\alpha(t,x)| \le v_{max} := \max\left\{ v_R,\ \delta \sup_{t,x} \kappa_B(t,x)(\overline{a_P}-\underline{a_B}) - v_R \right\} \tag{3.3}$$

Plugged into the boundary conditions (2.6) this leads to the following estimate.

Corollary 3.3. *For any smooth physical solution (u, a) of (FBP) we have*

$$|\partial_x a(t,x)| \le \frac{v_{max}\overline{a_P}}{D} \qquad \text{for each } (t,x) \in \mathcal{L}Q_T$$

where $\mathcal{L}Q_T$ is the lateral boundary of Q_T.

If we know which characteristic families of the hyperbolic part are the leading ones it is possible to write the boundary velocities in terms of the monomer density only. We therefore start with the strictly hyperbolic case where the initial conditions for a at the boundary points are such that the velocities of the filament tips at the membrane are mutually distinct. The equations for the boundary velocities then read

$$\dot{l}(t) = \lambda^{\alpha_l}(a(t,l(t))), \qquad \dot{r}(t) = \lambda^{\alpha_r}(a(t,r(t))) \qquad \text{for } t \in (0,T).$$

3.1 The strictly hyperbolic case with constant coefficients

Besides the assumption of strict hyperbolicity at the boundary we assume for the moment that all reaction parameters are constant and satisfy Cond. 3.1. Moreover, we assume the initial conditions to be such that at the initial boundary points all characteristic velocities λ^α are mutually different, and we denote the leading characteristic families by α_l and α_r.

For appropriate initial data, the unique solution results as a fixed point from the linearized system

$$\partial_t u + \partial_x(\Lambda A u) = 0 \qquad \text{in } (0,T)\times Q_T(A) \tag{3.4}$$

$$\partial_t a - D\partial_{xx} a + c\cdot U a = \tilde{c}\cdot U \qquad \text{in } Q_T(a) \tag{3.5}$$

with U and A being prescribed functions. For the parabolic equation we assume boundary conditions (2.6) and solve it on Q_T with boundary curves determined by $\lambda^{\alpha_{r/l}}(a)$. The hyperbolic equation is solved on the domain determined by plugging A into the equations for the boundary curves.

Now, the hyperbolic part is just a linear characteristic boundary value problem with diagonal velocity matrix and can be solved directly. The parabolic free boundary problem is more involved and is solved by again decoupling the unknown functions, the density a and the boundary curves r and l, from each other. First we note

Proposition 3.4. *Let $\beta \in (0,1)$, assume given boundary curves l, r belonging to $C^{1+\frac{1+\beta}{2}}([0.T])$ such that $r(t)-l(t) \ge d > 0$ for all $t \in [0,T]$. Let $U \in C^{0+\beta,P}(\overline{Q_T};\mathbb{R}^4)$ be given (for definition and properties of parabolic Hölder spaces see the appendix). Then, for any initial data $a_0 \in C^{2+\beta}([0,L])$ satisfying the compatibility conditions*

$$a_B \le a_0(x) \le a_P \qquad \text{for each } x \in [0,L] \tag{3.6a}$$

$$D\frac{d}{dx}a_0(0) + \dot{l}(0)a_0(0) = 0, \qquad D\frac{d}{dx}a_0(L) + \dot{r}(0)a_0(L) = 0 \tag{3.6b}$$

problem (3.5), (2.6) has a unique solution $a \in C^{2+\beta,P}(\overline{Q_T})$, and there exists $C > 0$, depending only on l, r, D, β, $\|c\cdot U\|_{C^{0+\beta,P}}$ such that

$$\|a\|_{C^{2+\beta,P}} \le C\left(\|\tilde{c}\cdot U\|_{C^{0+\beta,P}} + \|a_0\|_{C^{2+\beta}}\right).$$

The proof of this theorem relies on Schauder estimates for parabolic problems solved in Hölder spaces. It is a special case of Thm. 5.18 in [14] with slight modifications of the notation as discussed in [8]. We therefore omit the proof here.

If on the other hand $a \in C^1([0,T]\times\mathbb{R})$, bounded with bounded derivatives, is given then the boundary curves described by initial value problems of the form

$$\dot{g}(t) = c_1 a(t, g(t)) + c_2, \qquad g(0) = x_0$$

are continuously differentiable with uniformly Lipschitz continuous derivatives. If the given monomer density a is of class $C^{2+\beta,P}$ then these curves are of class $C^{2+\frac{\beta}{2}}$ and bounded in this space.

The parabolic free boundary problem is now transformed to a fixed domain $\tilde{Q}_T = (0,T)\times(0,L)$ by the coordinate transformation

$$\tau = t, \qquad \xi = \frac{L}{r(t)-l(t)}(x - l(t)).$$

In these coordinates the equation for the rescaled monomer density $\tilde{a}(\tau,\xi) = a(t(\tau,\xi), x(\tau,\xi))$ reads

$$\partial_\tau \tilde{a} - \frac{L^2 D}{(r-l)^2}\partial_{\xi\xi}\tilde{a} - \frac{L}{r-l}\left(\frac{\xi}{L}(\dot{r}-\dot{l}) + \dot{l}\right)\partial_\xi \tilde{a} + \tilde{\varphi}\tilde{a} = \tilde{f} \tag{3.7}$$

where $\tilde{\varphi}(\tau,\xi) = \varphi(t(\tau,\xi), x(\tau,\xi))$ and $\tilde{f}(\tau,\xi) = f(t(\tau,\xi), x(\tau,\xi))$ are the rescaled versions of $\varphi := c\cdot U$ and $f := \tilde{c}\cdot U$, respectively, and l and r are now merely virtual boundary curves given by

$$\dot{l}(\tau) = \lambda^{\alpha_l}(\tilde{a}(\tau,0)), \qquad l(0) = 0 \tag{3.8}$$

$$\dot{r}(\tau) = \lambda^{\alpha_r}(\tilde{a}(\tau,L)), \qquad r(0) = L \tag{3.9}$$

and only act as coefficients in this equation.

The boundary conditions for the parabolic equation are turned into

$$DL\partial_\xi \tilde{a}(\tau,0) + \dot{l}(\tau)\tilde{a}(\tau,0) = 0 = DL\partial_\xi \tilde{a}(\tau,L) + \dot{r}(\tau)\tilde{a}(\tau,L),\ \tau\in(0,T). \tag{3.10}$$

By inserting (3.8) and (3.9) into (3.10) we obtain effectively nonlinear boundary conditions for $\tilde{a}$. We denote the initial data by a_0 and emphasize that at $\tau = 0$, the rescaled and the physical coordinates coincide.

Analogously to Prop. 3.4 we find

Proposition 3.5. *Given $\beta\in(0,1)$, φ, $f\in C^{0+\beta,P}(\overline{Q_T})$, and l, r of class $C^{1+\frac{1+\beta}{2}}([0,T])$ such that $r(\tau)-l(\tau)\geq d>0$, for any initial conditions $a_0\in C^{2+\beta}([0,L])$, problem (3.7), (3.10) has a unique solution $\tilde{a}\in C^{2+\beta,P}(\overline{\tilde{Q}_T})$, and there exists a constant $C>0$, depending only on*

$$T,\ \beta,\ \|l\|_{C^{1+\frac{1+\beta}{2}}},\ \|r-L\|_{C^{1+\frac{1+\beta}{2}}}, \|\varphi\|_{C^{0+\beta,P}}, L, \text{ and } D,$$

such that

$$\|\tilde{a}\|_{C^{2+\beta,P}(\overline{\tilde{Q}_T})} \leq C\left(\|f\|_{C^{0+\beta,P}(\overline{Q_T})} + \|a_0\|_{C^{2+\beta}}\right). \tag{3.11}$$

Moreover, the boundary gradient obeys the uniform estimates

$$|\partial_\xi \tilde{a}(\tau,\xi)| \le \frac{V\,(L+2VT)}{LD} a_P \qquad \text{for } \tau \in [0,T],\ \xi = 0, L$$

where

$$V := \max\left\{ \|\dot{l}\|_{C^0}, \|\dot{r}\|_{C^0} \right\}$$

is the maximal velocity of the virtual boundary curves.

To apply Thm. 5.18 in [14] a little caution is necessary. One has to show the sufficient regularity of the coefficient functions of the transformed problem, in particular those in the diffusion and the drift term in (3.10) and in the boundary conditions. For finite times they indeed satisfy all the requirements of Thm. 5.18 in [14] which can be shown by explicite calculations given in detail in [8].

Remark 3.6. *The proposition remains valid also for boundary conditions*

$$\begin{aligned} DL\partial_\xi \tilde{a}(\tau,0) + \dot{l}(\tau)\tilde{a}(\tau,0) &= g(\tau,0), \qquad \tau \in (0,T) \\ DL\partial_\xi \tilde{a}(\tau,L) + \dot{r}(\tau)\tilde{a}(\tau,L) &= g(\tau,L), \qquad \tau \in (0,T). \end{aligned}$$

where g is of class $C^{1+\beta,P}$. Upon, if necessary, adapting the compatibility conditions for the initial and boundary values at the corner points, we obtain the same assertion with (3.11) being replaced by

$$\|\tilde{a}\|_{C^{2+\beta,P}(\overline{\tilde{Q}_T})} \le C\left(\|f\|_{C^{0+\beta,P}(\overline{Q_T})} + \|a_0\|_{C^{2+\beta}} + \|g\|_{C^{1+\beta,P}} \right).$$

So in summary:

1. given boundary curves of class $C^{1+\frac{1+\beta}{2}}$ (and end densities of class $C^{0+\beta,P}$) we find a unique solution $\tilde{a}$ to the parabolic boundary value problem on the transformed domain which is of class $C^{2+\beta,P}$, and
2. conversely, given a solution $\tilde{a}$ to the parabolic equation having regularity $C^{2_x,1_t}$ we obtain boundary curves which are of class $C^{1,1}$.

This allows us for sufficiently small times T to construct a contraction in the space

$$\begin{aligned} X_T &= C^{2_x,1_t}([0,T]\times[0,L]) \times \left(C^{1+\frac{1+\beta}{2}}([0,T])\right)^2, \\ \|(\tilde{a},l,r)\|_{X_T} &:= \|\tilde{a}\|_{C^{2_x,1_t}} + \|l\|_{C^{1+\frac{1+\beta}{2}}} + \|r-L\|_{C^{1+\frac{1+\beta}{2}}} \end{aligned}$$

mapping the prescribed functions $\tilde{a}$, l and r to the solution $\tilde{a}'$ of the parabolic boundary value problem (3.7), (3.10) with boundary curves l, r and the solutions l', r' of the boundary curve equations (3.8), (3.9) with right hand sides determined by $\tilde{a}$, respectively.

To do so, let a_0 and U be given. Then, the boundary curves have initially the same velocity (determined by the values of a_0 at the corner points).

Consider now two sets of prescribed functions $(\tilde{a}_1, l_1, r_1)$ and $(\tilde{a}_2, l_2, r_2)$ satisfying the same initial data. Then, the difference

$$(w,\sigma,\rho) := (\tilde{a}_1', l_1', r_1') - (\tilde{a}_2', l_2', r_2')$$

of the solutions has the initial conditions $(0,0,0)$ and in addition $\dot\sigma(0)=\dot\rho(0)=0$. Moreover,

$$\begin{aligned}\partial_\tau w &= \frac{L^2 D}{(r_2-l_2)^2}\partial_{\xi\xi} w + \frac{L}{r_2-l_2}\left(\frac{\xi}{L}(\dot r_2-\dot l_2)+\dot l_2\right)\partial_\xi w - \tilde\varphi w \\ &\quad + L^2 D\Theta\partial_{\xi\xi}\tilde a_1' + (\Sigma_2-\Sigma_1)\partial_\xi \tilde a_1' \end{aligned} \tag{3.13}$$

where

$$\Theta(\tau) := \frac{(r_1(\tau)-l_1(\tau))^2-(r_2(\tau)-l_2(\tau))^2}{(r_1(\tau)-l_1(\tau))^2(r_2(\tau)-l_2(\tau))^2} \tag{3.14}$$

$$\Sigma_i(\tau) := \frac{L}{r_i(\tau)-l_i(\tau)}\left(\frac{\xi}{L}(\dot r_i(\tau)-\dot l_i(\tau))+\dot l_i(\tau)\right), \quad i=1,2. \tag{3.15}$$

The boundary conditions for w read

$$\begin{aligned} DL\partial_\xi w(\tau,0)+\dot l_2(r_2-l_2)w(\tau,0) &= \left(\dot l_2(r_2-l_2)-\dot l_1(r_1-l_1)\right)\tilde a_1'(\tau,0) \\ &=: g(\tau,0) \qquad (3.16a)\\ DL\partial_\xi w(\tau,L)+\dot r_2(r_2-l_2)w(\tau,L) &= (\dot r_2(r_2-l_2)-\dot r_1(r_1-l_1))\,\tilde a_1'(\tau,L) \\ &=: g(\tau,L). \qquad (3.16b)\end{aligned}$$

Finally, the difference of the virtual boundary curves are determined by

$$\dot\sigma(\tau)=\kappa^0(\tilde a_2(\tau,0)-\tilde a_1(\tau,0)), \qquad \dot\rho(\tau)=\kappa^L(\tilde a_2(\tau,L)-\tilde a_1(\tau,L)) \tag{3.17}$$

where κ^0 and κ^L are constants of the form $\pm\delta\,\kappa_{B/P}$.

Using the bounds on the solutions, we conclude that

$$\begin{aligned}\|w\|_{C^{2_x,1_t}} &\le T^{\frac{\beta}{2}} T_0^{\frac{2+\beta}{2}}\|w\|_{C^{2+\beta,P}} \\ &\le CT^{\frac{\beta}{2}}\left(\|l_1-l_2\|_{C^{1+\frac{1+\beta}{2}}}+\|r_1-r_2\|_{C^{1+\frac{1+\beta}{2}}}\right) \\ &\le CT^{\frac{\beta}{2}}\|(\tilde a_1,l_1,r_1)-(\tilde a_2,l_2,r_2)\|_{X_T}\end{aligned}$$

where the constant C can be taken from (3.11) for some fixed time T_0. In that case, the above estimate holds for all times $T\le T_0$.

Similarly, we find for the difference of the boundary curve solutions

$$\begin{aligned}\|\sigma\|_{C^{1+\frac{1+\beta}{2}}} &= \|\sigma\|_{C^0}+\|\dot\sigma\|_{C^0}+H\ddot{o}l_{\frac{1+\beta}{2}}(\dot\sigma) \;\le\; (T^2+T+1)T^{\frac{1-\beta}{2}}Lip(\dot\sigma) \\ &\le \delta\,\kappa_B(T^2+T+1)T^{\frac{1-\beta}{2}}\|\tilde a_1-\tilde a_2\|_{C^{2_x,1_t}} \\ &\le C\;T^{\frac{1-\beta}{2}}\|(\tilde a_1,l_1,r_1)-(\tilde a_2,l_2,r_2)\|_{X_T},\end{aligned}$$

and literally the same estimate applies to ρ.

By choosing T sufficiently small, we therefore obtain that the solution operator is a contraction from the closed bounded subset

$$\begin{aligned}\mathcal{B}_T = \Big\{(\tilde a,l,r)\in X_T \;\Big|\;\; & \|r-L\|_{C^0}\le\varepsilon_1, \|\dot r-v_{r0}\|_{C^0}\le\varepsilon_2, H\ddot{o}l_{\frac{1+\beta}{2}}(\dot r)\le\Lambda_1, \\ & \|l\|_{C^0}\le\varepsilon_1, \|\dot l-v_{l0}\|_{C^0}\le\varepsilon_2, H\ddot{o}l_{\frac{1+\beta}{2}}(\dot l)\le\Lambda_1, \\ & a_B\le\tilde a(\tau,\xi)\le a_P, \|\tilde a\|_{C^{2_x,1_t}}\le\Upsilon_1, \\ & (\tilde a(0,\cdot),l(0),r(0))=(a_0,0,L),\;\dot l(0)=v_{l0},\;\dot r(0)=v_{r0}\Big\}\end{aligned}$$

of X_T into itself, more precisely, even into the precompact set $\mathcal{B}_T \cap Y_T$ where

$$Y_T = C^{2+\beta,P}(\overline{\tilde{Q}_T}) \times \left(C^{1+1}([0,T])\right)^2 \hookrightarrow\hookrightarrow X_T$$

is a compact subspace of X_T if equipped with the natural norm

$$\|(\tilde{a},l,r)\|_{Y_T} := \|\tilde{a}\|_{C^{2+\beta,P}} + \|l\|_{C^{1,1}} + \|r-L\|_{C^{1,1}}.$$

The unique fixed point of this contraction is our solution $(\tilde{a},l,r)$ of the parabolic free boundary problem for given end densities U. This solution is bounded in Y_T. The transformation back to the physical domain Q_T does not lower the regularity of the solution.

So far we have not yet dealt with the hyperbolic equations besides having inserted a given solution U as coefficient function into the parabolic free boundary problem. We required U to be of class $C^{0+\beta,P}$ in order to find a $C^{2+\beta,P}$-solution a. Conversely, given a monomer density A of class $C^{2_x,1_t}$ and thereby $C^{2_x,1_t}$-velocity fields

$$\lambda^\alpha(t,x) = \kappa^\alpha A(t,x) + k^\alpha,$$

the hyperbolic equations possess unique C^1-solutions u^α. These can be shown to satisfy

$$\begin{aligned}\|u^\alpha\|_{C^1} \;\leq\; & M_0^\alpha\left(1+\kappa^\alpha\|\partial_x A\|_{C^0}\right)\mathcal{E}^\alpha(2T) \\ & + \left[M_1^\alpha + M_0^\alpha\kappa^\alpha\|\partial_{xx}A\|_{C^0}T\mathcal{E}^\alpha(2T)\right](1+v_{max})\mathcal{E}^\alpha(2T)\end{aligned}$$

where v_{max} is given by (3.3),

$$M_0^\alpha := \max_{x\in[0,L]}|u^\alpha(0,x)|, \qquad M_1^\alpha := \max_{x\in[0,L]}|\partial_x u^\alpha(0,x)|,$$

and where $$\mathcal{E}^\alpha(t) := \exp\left[\kappa^\alpha\|\partial_x A\|_{C^0}t\right]$$

provides an upper bound for the growth of end densities according to the inhomogeneities of the velocity field.

Now we have constructed a solution $(\tilde{a},l,r)\in X_T$ for the transformed parabolic free boundary problem for given end densities $U^\alpha \in C^{0+\beta,P}$ and conversely found a C^1-solution to the hyperbolic Cauchy problem for prescribed monomer density $A \in C^{2_x,1_t}$.

Using the above estimates for the solutions we can now assert the existence of a unique solution to the full problem as fixed point of a contraction operator assigning to given $(\tilde{A},l,r) \in X_T$ and $U \in \left(C^{0+\beta,P}\right)^4$ the respective solutions $(\tilde{a},l',r') \in Y_T$ and $u \in \left(C^1\right)^4$ of the linearized problem. So this operator maps

$$V_T := X_T \times \left(C_b^{0+\beta,P}(E_T)\right)^4 \to Y_T \times \left(C^1([0,T]\times\mathbb{R})\right)^4 =: W_T \hookrightarrow\hookrightarrow V_T.$$

where $C_b^{0+\beta,P}(E_T)$ denotes the space of bounded $C^{0+\beta,P}$ functions with uniformly bounded Hölder constants on the strip $E_T := [0,T]\times\mathbb{R}$.

The estimates assure that for sufficiently small T, this operator maps

$$\begin{aligned}\mathcal{C}_T \;=\; & \Big\{(\tilde{a},l,\tilde{r},u) \in \mathcal{B}_T \times \Big(C_b^{0+\beta,P}(E_T)\Big)^4 \;\Big|\; a^{BP} \leq \tilde{a} \leq a_P, \|\partial_\xi\tilde{a}\|_{C^0} \leq \Upsilon_0, \\ & \dot{l}(\tau) = c_1^1\tilde{a}(\tau,0) + c_2^1,\ \dot{r}(\tau) = c_1^4\tilde{a}(\tau,L) + c_2^4 \quad \text{for } \tau\in[0,T], \\ & \max_{\alpha=1,\dots,4}\|u^\alpha\|_{C^{0+\beta,P}} \leq \Upsilon_2, \\ & \operatorname{supp} u \subset [0,T]\times\left[-\frac{L}{4},\frac{5}{4}L\right],\ u(0,\cdot)=u_0,\ a(0,\cdot)=a_0\Big\}\end{aligned}$$

into $\mathcal{C}_T \cap W_T$ if the constants in the definition of $\mathcal{C}_T$ are appropriately chosen.

Again we assume to be given two quadruples

$$(\tilde{a}_i, l_i, r_i, u_i) \in \mathcal{C}_T, \qquad (i = 1,\, 2)$$

corresponding to the same (compatible) initial data. Then

$$(w, \sigma, \rho, \omega) := (\tilde{a}_2', l_2', r_2', u_2') - (\tilde{a}_1', l_1', r_1', u_1')$$

satisfies

$$\begin{aligned}\partial_\tau w \;&= \frac{L^2 D}{(r_2 - l_2)^2}\partial_{\xi\xi} w + \frac{L}{r_2 - l_2}\left(\frac{\xi}{L}(\dot{r}_2 - \dot{l}_2) + \dot{l}_2\right)\partial_\xi w - \tilde{\varphi}_2 w \\ &\quad + L^2 D\Theta\partial_{\xi\xi}\tilde{a}_1' + (\Sigma_2 - \Sigma_1)\partial_\xi \tilde{a}_1' - (\tilde{\varphi}_2 - \tilde{\varphi}_1)\tilde{a}_1' + (\tilde{f}_2 - \tilde{f}_1), \qquad (3.18)\end{aligned}$$

where Θ and Σ_i are defined by (3.14) and (3.15), respectively.

The boundary conditions for w are given by (3.16a,b), and the virtual boundary curves are again determined from (3.17).

For the components ω^α of the difference in the end densities we obtain

$$\begin{aligned}\omega^\alpha(t,x) \;&= u_0^\alpha(y_2^\alpha(0;t,x))\;\exp\left[-\int_0^t \partial_x \lambda_2^\alpha(s, y_2^\alpha(s;t,x))\mathrm{d}s\right] \\ &\quad + u_0^\alpha(y_1^\alpha(0;t,x))\;\exp\left[-\int_0^t \partial_x \lambda_2^\alpha(s, y_2^\alpha(s;t,x))\mathrm{d}s\right]. \qquad (3.19)\end{aligned}$$

Here, $y^\alpha(s;t,x)$ denotes the spatial position at time s of the α^{th} characteristic curve passing through (t,x) and the subscripts $i = 1,\, 2$ refer to the characteristic curves and velocity fields according to the given scaled monomer densities $\tilde{a}_i$ and the corresponding boundary curves l_i and r_i, respectively.

Of course, again all initial conditions for the differences and the initial velocity differences $\dot{\sigma}(0)$ and $\dot{\rho}(0)$ are identically zero.

By choosing the time T sufficiently small we can again use the estimates on the solution of the rescaled parabolic problem for given end densities on the one hand and the explicite integral representation of the solution to the hyperbolic part for given velocity fields on the other hand to assure that our solution operator is indeed a contraction on $\mathcal{C}_T$. The detailed calculations are carried out in [8].

We thus arrive at the main result of this section

Theorem 3.7. *Given $\beta \in (0,1)$ and $L > 0$, let the initial conditions*

$$u_0 \in C^2([0,L]) \qquad \text{and} \qquad a_0 \in C^{2+\beta}([0,L]) \qquad (3.20)$$

satisfy the compatibility conditions (3.6) and $a_B \le a_0 \le a_P$. Assume further the conditions (3.1) on the end densities and for some $\varepsilon > 0$ that:

$$\begin{aligned}&|\lambda^1(a_0(0)) - \lambda^2(a_0(0))| \ge \varepsilon \;\text{ or }\; u^2 = 0 \text{ on } [0,\varepsilon) \qquad \text{or} \quad u^1 = 0 \text{ on } [0,\varepsilon) \\ &|\lambda^3(a_0(L)) - \lambda^4(a_0(L))| \ge \varepsilon \;\text{ or } u^3 = 0 \text{ on } (L-\varepsilon, L] \;\text{ or } u^4 = 0 \text{ on } (L-\varepsilon, L].\end{aligned}$$

Then, there exists a time $T^* > 0$, depending only on

$$\beta,\; L,\; D,\; \kappa_{B/P},\; a_{B/P},\; v_R,\; \delta,\; \|u_0\|_{C^0},\; \|u_0'\|_{C^0},\; \|u_0''\|_{C^0},\; \|a_0\|_{C^{2+\beta}}, \text{ and } \varepsilon$$

such that for each $T \in (0, T^*)$ the problem (FBP) has a unique solution.

3.2 Notes on some relaxed assumptions

Next we want to consider the case of variable coefficients. All the theorems on the unique solvability and the estimates for the linearized problems remain valid if the reaction parameters are allowed to vary smoothly within the range specified by Cond. 3.1. In general, the time T^* in Thm. 3.7 will then be smaller than in the constant coefficient case. Moreover, the conditions on the initial data have to be adapted to the non-uniform nature of the parameters in order to ensure compatibility at the corners, initial strict hyperbolicity, and the monomer concentration to be in the physiological range. For example, condition $a_B \leq a_0 \leq a_P$ has to be understood pointwise and in the hypotheses of Thm. 3.7, the velocities λ^α do not only depend on a but also explicitely on x and t.

All calculations leading to the contraction argument for the decoupled problems remain basically the same. The additional terms entering the hyperbolic equations due to nontrivial derivatives of the parameters simply lead to some additional constants in the estimates, depending only on the norms of $\kappa_{B/P}$ and $a_{B/P}$ in the space $C^{2_x,1_t}([0,T]\times\mathbb{R})$.

Second we want to relax the assumption of strict hyperbolicity at the boundary. If the leading characteristic family remains the same, there will be no changes for the solvability of the problem.

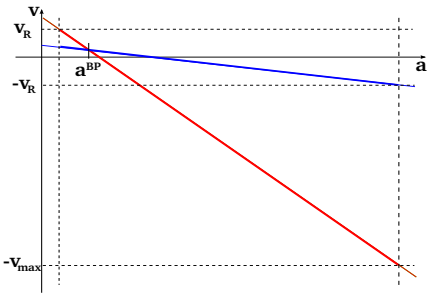

Figure 1: Possible boundary velocities for the left boundary depending on a; *red*: $-v_B(a)$, *blue*: $v_P(a)$. The slopes and the position of the endpoints on the abscissa may vary if the coefficients are variable.

If however, the outer characteristic curves of two different end densities cross at the boundary, the boundary curves will in general have a kink at this point and are therefore merely Lipschitz continuous. This does heavily affect the possible regularity of a which cannot be expected to be continuously differentiable up to the boundary if the boundary velocities $\dot{l}$ and $\dot{r}$ are not assumed to be continuous.

Since we are only concerned with physical solutions we have to consider just two possible switches of the leading characteristic families per side. For the left boundary these are the following cases.

1. The characteristic family u^2 takes over the lead from u^1 at $t = t_0$. Then
$$\lambda^1 > \lambda^2 \quad \text{thus} \quad a(t,x) < a^{BP}$$
on some parabolic cylinder $\mathrm{Cyl}_r(t_0, l(t_0)) \cap Q_T$ where
$$a^{BP} = \frac{2\frac{v_R}{\delta} + \kappa_B a_B - \kappa_P a_P}{\kappa_B - \kappa_P}$$
is the value of the monomer density at which $v_B = -v_P$. We may w.l.o.g. assume the strict inequality also to be satisfied in the limit
$$\lim_{t \nearrow t_0} a(t, l(t)) < a^{BP}(t_0, l(t_0))$$

since otherwise the velocity would not exhibit a jump. Fig. 1 shows that in this case, both characteristic velocities are positive.

2. If u^2 ceases to be the leading characteristic family and is replaced by u^1 at $t = t_0$ we have $a > a^{BP}$ in some parabolic cylinder below $(t_0, l(t_0))$. We now have three generic cases for the signs of the limit values of the velocities at $(t_0, l(t_0))$:

$$(i)\ \ 0 < \lambda^1 < \lambda^2 \quad \text{or} \quad (ii)\ \lambda^1 < 0 < \lambda^2 \quad \text{or} \quad (iii)\ \lambda^1 < \lambda^2 < 0$$

as sketched in Fig. 2.

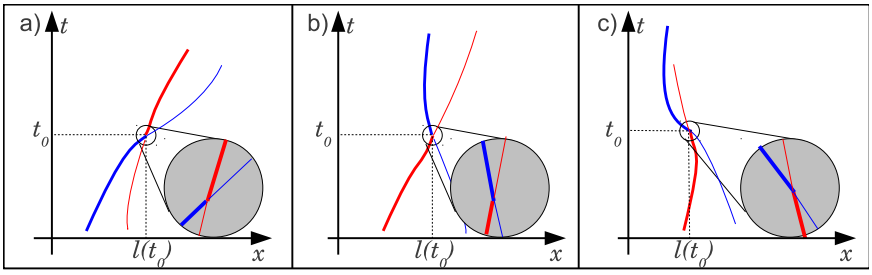

Figure 2: Possible behavior of the left boundary curve (thick line) around a point $(t_0, l(t_0))$ where the outer characteristics of u^1 and u^2 cross. *Blue* codes for $l^1(t)$, *red* for $l^2(t)$. The grey circles show a zoom into the vicinity of the crossing points. Picture a) corresponds to case 1. Note that case 2.(i) has a similar shape with colors being exchanged. Pictures b) and c) sketch the situation of cases 2.(ii) and 2.(iii), respectively.

We now have a free boundary problem as above with t_0 as initial time but with data not being compatible at the corner points. For prescribed boundary curves and end densities, the solution of the parabolic equation is only uniformly continuous with bounded first spatial derivative $\partial_\xi \tilde{a}$ for $t \geq t_0$. This derivative however has a discontinuity at the corner points, and the second spatial and first temporal derivatives of a have discontinuities of the order

$$\sup_\xi(|\partial_\tau \tilde{a}|, |\partial_{\xi\xi} a|) \sim \frac{1}{\sqrt{\tau - t_0}} \qquad \text{as } \tau \searrow t_0$$

at these points. In particular, $\partial_\tau \tilde{a}$ and $\partial_{\xi\xi} \tilde{a}$ belong to $L_p(t_0, t_0 + T;\, L_\infty(0,\, L))$ for any $p \in [1, 2)$.

So for piecewise differentiable prescribed virtual boundary curves with derivatives $\dot{l}$ and $\dot{r}$ being piecewise Hölder continuous of exponent $(1+\beta)/2$ with discontinuities at times t_* we obtain a rescaled monomer density $\tilde{a}$ that is even of class $C^{2+\beta,P}$ on each open subset of Q_T not containing lines $\{t = t_*\}$. Extending this density suitably to some function $\bar{a}$ on $[0, T] \times \mathbb{R}$ we obtain

$$\bar{a} \in C^0([0, T] \times \mathbb{R}) \cap C^1((0, T) \backslash \mathcal{N}; C^2(\mathbb{R})) \tag{3.21}$$

where $\mathcal{N}$ is the discrete set of points t_* where the boundary velocities jump. In case the assumption of $\mathcal{N}$ being discrete is dropped we still obtain

$$\bar{a} \in C^0([0, T] \times \mathbb{R}) \cap L_\infty(0, T; C^{0+1}(\mathbb{R})). \tag{3.22}$$

If such a monomer density is prescribed we can solve (3.8) and (3.9) in the sense of Carathéodory (cf. Chapter 2 in [3]) and obtain absolutely continuous solutions l and r which are unique due to the spatially uniform Lipschitz bounds of the velocity fields. These solutions are uniformly Lipschitz continuous and apart from the points of discontinuity of the coefficient functions are continuously differentiable.

Finally, by the theory developed in [4], specifically Prop. II.1 and Corollary II.1 therein, the hyperbolic equations have unique solutions u^α in the space of signed Radon measures for given velocity fields

$$\lambda^\alpha \in L_1(0,T;W_\infty^{1,loc}) \hookleftarrow L_\infty(0,T;C^{0+1}(\mathbb{R}))$$

the latter being the space to which $\bar{a}$ belongs. For our particular situation with $\lambda^\alpha \in L_\infty(0,T;W_\infty^{1,loc}(\mathbb{R})) \cap L_p(0,T;W_\infty^{2,loc}(\mathbb{R}))$ these u are differentiable with bounded derivatives if the initial conditions are continuously differentiable with compact support.

With these preliminaries we can again construct a contraction. We assume that the outer characteristics on at least one boundary cross at $t = t_0 = 0$. Replace V_T from Subsection 3.1 by

$$\begin{aligned}\tilde{V}_T \ := &\left(C^0([0,T]\times[l_-,r_+]) \cap L_\infty(0,T;W_\infty^1(l_-,r_+)) \cap L_{p_0}(0,T;W_\infty^2(l_-,r_+))\right)\\ &\times \left(C^{1+\beta_0}([0,T])\right)^2 \times \left(C^{0+\beta_0,P}([0,T]\times[l_-,r_+])\right)^4,\end{aligned}$$

where T is chosen sufficiently small to prevent the outer characteristic curves from crossing again for $0 < t \leq T$ and where $p_0 \in [1,2)$, $\beta_0 \in (\frac{1}{2},1)$ are freely chosen. Moreover, let l_- be sufficiently small and r_+ sufficiently large to guarantee $Q_T \subset (0,T)\times(l_-,r_+)$. The monomer density lying in the above spaces therefore means, that some suitable (spatial) extension $\bar{a}$ of a belongs to these spaces. Again, u can trivially be extended to the whole real line.

W_T from Subsection 3.1 is replaced by

$$\begin{aligned}\tilde{W}_T \ := &\left(C^0([0,T]\times[l_-,r_+]) \cap L_\infty(0,T;W_\infty^1(l_-,r_+)) \cap L_{p_1}(0,T;W_\infty^2(l_-,r_+))\right)\\ &\times \left(C^{1+\beta 1}([0,T])\right)^2 \times \left(W_\infty^1([0,T]\times[l_-,r_+])\right)\end{aligned}$$

with $\beta_1 p_0 < 1$, $p_0 < p_1 < 2$ and $\beta_1 > \beta_0$.

These choices together with the Lebesgue- and Hölder scales guarantee the contractivity of the solution operator on some closed bounded subset of $\tilde{V}_T$ for sufficiently small times T and therefore the existence of a unique solution.

3.3 Simulation of the free boundary problem

Having shown the well-posedness of the free boundary problem (FBP) for small times we are now interested in the behavior of the cell boundaries and the displacement of the cytoskeleton upon certain deviations of the parameters from the symmetric setting which led to the steady state solutions introduced in [7] and describing a resting cell.

We will change the critical concentrations $a_{B/P}$ and the reaction rate constants $\kappa_{B/P}$. Varying $a_{B/P}$ accounts for changes in the affinity of actin monomers to the respective filament ends which may be mediated by sequestering agents such as ADF/cofilin ([12]), profilin or thymosin-β_4 (cf. [16]). An alteration of $\kappa_{B/P}$ reflects a catalytic activity of enzymes like membrane bound

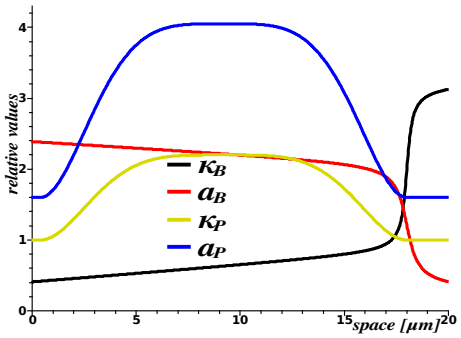

Figure 3: Typical spatial variations of κ_B, κ_P and a_B and a_P in units of their respective steady state values. In this example, barbed end polymerization is strongly enhanced close to the right cell boundary whereas boosted pointed end depolymerization in the center of the cell provides additional monomers. For the simulations, different combinations of these variations were examined.

formins (cf. [9]). The basis parameters we use as reference values are taken from the in-vitro measurements conducted in [18].

Many of these actin binding proteins are regulated by GTPases of the Rho-family (reviewed in [11]), a process we do not explicitely model here. Instead we take plausible variations of the reaction parameters as shown in Fig. 3.

Another possible way of driving the cell out of its symmetric resting state is the localized supply of additional monomers which we also investigate in the simulations. Moreover, the effect of the monomer diffusion coefficient D, which varies between about $2\,\mu m^2 s^{-1}$ in dense actin gels and about $30\,\mu m^2 s^{-1}$ in pure cytosol (cf. [17]), is discussed.

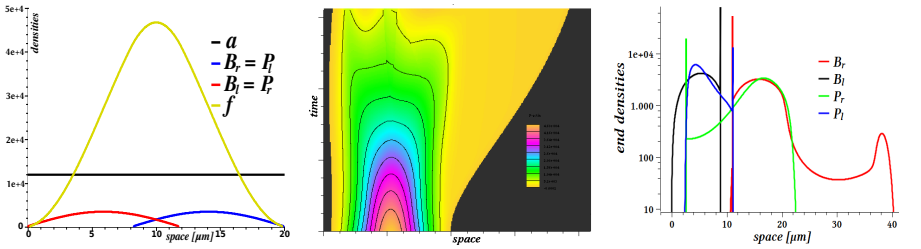

Figure 4: Simulations of an initially resting cell turning into motion upon some external stimulus (variations of reaction rate κ_B and critical concentration a_P as sketched in Fig. 3, κ_P and a_B being kept at their default values). *Left*: typical initial conditions for the monomer density (*black*), the filament end densities (*red, blue*) and the total F-actin density (*green*). *Middle*: temporal evolution of the F-actin density, *right*: filament end distributions after $t = 60\,s$. The Dirac-δ like peaks are not artefacts but resemble actin polymerization fronts as will be discussed in Sec. 4.

We start with symmetric initial conditions corresponding to a resting cell as depicted in Fig. 4, left. Any of the above mentioned variations let the right boundary move forward, thus mimicking the establishment of a lamellipodium. This is not surprising since the perturbations have been constructed such that barbed end polymerization is enhanced at the right boundary.

Nevertheless, there are striking differences in the dynamics of filamentous actin depending on the type of parameter variation.

The main differences lie in the initial velocities and the persistence of the boundary movement. Increased κ_B or the release of monomers close to the right boundary yield high initial velocities but after about ten seconds the velocity significantly drops due to monomer depletion.

Changing the critical concentrations $a_{B,P}$ leads to initially slower velocities but the motion is much more persistent as there is a permanent monomer supply by pointed end depolymerization and diffusion of monomers to the moving boundary.

The most pronounced effect results from combining the different perturbations. Of course, we only examine the initial stage of polarization of the cytoskeleton. Establishing a real lamellipodium would require in addition filament branching, nucleation of new and total depolymerization of old filaments, filament alignment, and mechanical forces.

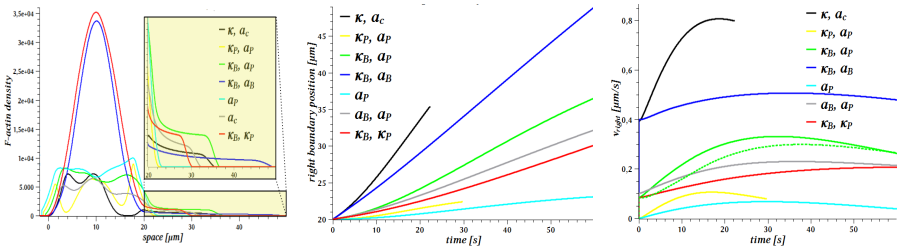

Figure 5: Simulation results for different types of parameter variations (according to Fig. 3) for $D = 30\,\mu m^2 s^{-1}$. Varied parameters are indicated in the legends (a_c stands for both, a_B and a_P). *Left*: F-actin concentration after $t = 60\,s$, except for variations of all parameters (*black*, $t = 23\,s$) and variation of κ_P, a_P (*yellow*, $t = 29\,s$). The zoom shows the F-actin distributions in the expanding part of the cell. Further the temporal evolution of r (*middle*) and the boundary velocity $\dot{r}$ (*right*; *dotted green* line: variation of κ_B and a_P at $D = 3\,\mu m^2 s^{-1}$) are shown.

In case some filament depolymerizes faster at its pointed end than it grows at the barbed end for a long time, the filament vanishes as soon as it is fully depolymerized. Since our model does not explicitely contain the filament lengths, we account for this situation by considering only times in the simulations before any of the F-actin concentrations drops below zero. This happens e.g. after about $30\,s$ in case of varied κ_P and a_P with κ_B and a_B being held constant. As depolymerization at the pointed ends is strongly enhanced without enhancing growth at the barbed ends, the filaments quickly shrink.

Related to our conjectures in [7], in case of additional monomer release close to the boundary, faster diffusion leads to a faster decrease of the local monomer concentration and thereby a quick drop of the boundary velocity. A sustained boundary movement is only observed upon changes in the reaction parameters which account for constantly increased barbed end polymerization in case of variations of κ_B and a_B or a permanent supply of additional monomers by depolymerization of pointed ends in case of increased κ_P and a_P.

As shown in Fig. 5 the strongest effect on the initial boundary velocity stems from variations of κ_B or a_B, and of course, this effect is most prominent if both are combined. Changes in κ_P or a_P yield a delayed effect since the production of monomers and their diffusion to the front takes some time. Here, a lower diffusion coefficient leads to a slower increase of the velocity. After some 60 seconds, this effect is however not significant anymore as a slightly shorter front region evolves which allows for the monomers to diffuse at a similar rate as is the case for high diffusion coefficients (Fig. 5, right).

The strongest effect of F-actin displacement to the right results from chang-

ing all parameters (black curves in Fig. 5). Only changing κ_B and a_B also yields a fast displacement of the right boundary. But in that case the filament density in the expanding portion of the cell (which is supposed to become the lamella) is rather small so we suspect that the velocity significantly drops as soon as the membrane is stretched and exerts a non-negligible force onto the growing barbed ends.

A very effective parameter variation proves to be a decreased affinity for monomers at the pointed ends resulting in larger a_P together with increased κ_B. Simply providing additional monomers for barbed end polymerization by increasing depolymerization at the pointed ends (changing κ_P and/or a_P) alone only yields a very slow movement of the boundary indicating that it is not likely to be sufficient to generate a quick polarization of the cytoskeleton.

4 Formation of polymerization fronts

Besides the fact that the crossing of characteristic curves at the boundary may reduce the regularity of solutions there may be other mechanisms preventing the solutions found in Sec. 3 from existing for large times. Simulations of the full system indicated the emergence of sharp peaks in the end densities accompanied by steep gradients in the monomer concentration. Together with the findings about traveling wave solutions for a related system analyzed in [6] this leads to the question whether some kind of shock solutions exist and, if so, how these might look like.

4.1 Dirac peaks with continuous monomer concentration

We consider the full system (2.2), (2.3) and an actin filament density as indicated in Fig. 6. An equal number of right and left oriented filaments is distributed symmetrically around the center of the cell located the origin. The barbed ends of either orientation are concentrated at the membrane which is located at $\pm(x_0 + l_0)$. The corresponding pointed ends concentrate at $\mp x_0$.

For the monomers, we assume

$$a_P^0 := a_P - \frac{v_R}{\delta\,\kappa_P} \tag{4.1}$$

in the center of the cell. This is just the monomer density at which the pointed end velocity $v_P(a)$ vanishes. So the pointed ends do not move but constantly produce monomers by depolymerization. At the boundary points we now have a finite number of barbed ends and we assume

$$a_B^0 := a_B + \frac{v_R}{\delta\,\kappa_B} \tag{4.2}$$

at the boundary meaning that the barbed end velocity $v_B(a)$ is zero at the boundary. Our no-flux conditions for a have to be changed since the presence of a finite number filament tips directly at the membrane leads to a non-vanishing polymerization flux.

The velocities of the filament tips have to vanish at $\pm x_0$ and $\pm(x_0 + l_0)$ which leads to a necessary balance between monomer production by pointed and consumption by barbed ends:

$$\delta\,\kappa_P(a_P - a_P^0)p_0 = \delta\,\kappa_B(a_B^0 - a_B)b_0 \tag{4.3}$$

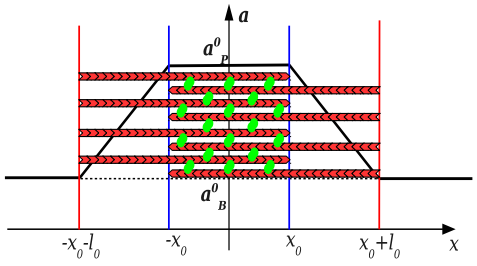

Figure 6: Cartoon of a measure valued steady state with actin filaments (*red*) and myosins (*green*) between them. The *black line* denotes the monomer density (outside the filaments extended as constant), bars denote the Dirac measures for the pointed (*blue*) and barbed (*red*) ends.

where p_0 and b_0 denote the masses of pointed and barbed ends concentrated in the Dirac peaks. If $p_0 = b_0$ we can compute the distance l_0 between the peaks since the diffusive flux $-D\partial_x a$ has to balance the polymerization flux. From

$$-D\partial_x a \equiv \frac{D}{l_0}\left(a_P^0 - a_B^0\right) \qquad \text{on } (x_0, x_0 + l_0)$$

we deduce

$$l_0 = \frac{D}{b_0 v_R}\left(a_P^0 - a_B^0\right) = \frac{D}{b_0 v_R}(a_P - a_B) - \frac{D}{b_0 \delta}\frac{\kappa_B + \kappa_P}{\kappa_B \kappa_P}. \tag{4.4}$$

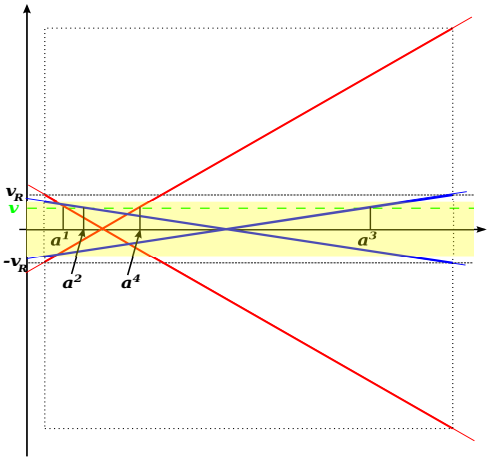

Figure 7: Barbed ($\pm v_B$, *red*) and pointed ($\pm v_P$, *blue*) end velocities depending on a and resulting values for a^α for a given positive velocity v of the profile. For v lying outside the range indicated by the yellow stripe there is no admissible value of a^2. The sides of the dashed rectangle depict the values a_B and a_P and $\pm v_{max}$, respectively.

Let us now look for solutions having a fixed shape moving at a constant velocity. That is, we look for solutions of the form

$$u^\alpha = u_0^\alpha \delta_{x^\alpha + vt}$$

where v is the velocity at which the profile moves and we choose $x^1 < x^2 < x^3 < x^4$. Further assume

$$a(x^\alpha + vt) =: a^\alpha(v) \qquad \text{such that} \qquad \lambda^\alpha(a^\alpha) = v \quad \text{for } \alpha = 1, \dots, 4$$

and interpolate according to the diffusion equation in between by solving the two point boundary value problem for the profile A between $x^\alpha + vt$ and $x^{\alpha+1} + vt$ ($\alpha = 1, 2, 3$). This profile has an unchanging shape and we can introduce

$$\xi := x - vt - x^\alpha \qquad \text{and} \qquad A(\xi) = A(x - vt - x^\alpha) := a(t, x).$$

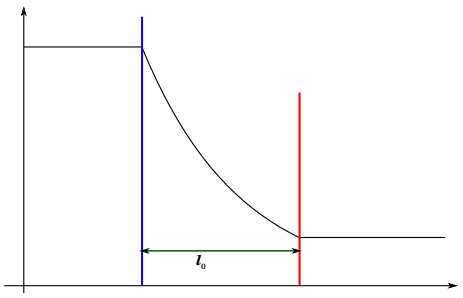

Figure 8: Sketch of a moving steady state profile with positive velocity v. The monomer concentration is drawn in *black*; the positions and masses of the DIRAC peaks for right oriented barbed ends (*red*) and left oriented pointed ends (*blue*) are shown as well. The distance l_0 here is given by (4.6).

Then, the shape A satisfies the problem

$$vA'(\xi) + DA''(\xi) = 0\ , \quad \text{with BC } A(0) = a^\alpha(v), \quad A(x^{\alpha+1} - x^\alpha) = a^{\alpha+1}(v).$$

The general solution of this problem is

$$A(\xi) = C_2 \exp\left[-\frac{v}{D}\xi\right] + \frac{C_1}{v}$$

with constants of integration C_1 and C_2 given by the boundary values. Moreover, the distances $l^\alpha := x^{\alpha+1} - x^\alpha$ ($\alpha = 1, 2, 3$) and the velocity v are free parameters to be determined from the flux conditions relating the diffusive flux $\pm DA'(x^\alpha \pm 0)$ to or from the shock positions to the production or consumption of monomers in the shocks due to (de)polymerization.

To avoid overly tedious calculations and notation we shall focus on the two rightmost peaks in Fig. 6, i.e. the right oriented barbed and left oriented pointed ends. Moreover, we assume both peaks to lie in the interior of the cell to avoid boundary effects.

Again denote the mass concentrated in the pointed and barbed end peaks by p_0 and b_0. Given a velocity v, from the boundary conditions for a we obtain the solution for the profile A of the monomer density between the peaks as

$$A(\xi) = a^3(v) - \frac{a^3(v) - a^4(v)}{1 - \exp\left[-\frac{v}{D}l^3\right]}\left(1 - \exp\left[-\frac{v}{D}\xi\right]\right).$$

With $\theta := v/v_R$, the flux conditions lead to

$$\theta(a^3(v) - a^4(v)) = (1-\theta)p_0 - (1+\theta)b_0 \tag{4.5}$$

$$l^3 = \frac{D}{v}\log\left[1 + \frac{a^3(v) - a^4(v)}{b_0}\frac{\theta}{1+\theta}\right]. \tag{4.6}$$

Here, (4.5) relates the velocity to the ratio of the numbers b_0 and p_0 of ends in the respective peaks, and (4.6) determines the distance between the peaks depending on the velocity and the absolute number of filament tips in the peaks. Fig. 8 shows a typical example of such a solution for positive velocities.

4.2 Shocks in the hyperbolic limit system

Formally letting $D = 0$ in (2.3) we obtain a hyperbolic system

$$\partial_t \begin{pmatrix} u^1 \\ u^2 \\ u^3 \\ u^4 \\ a \end{pmatrix} + \begin{pmatrix} \lambda^1 & 0 & 0 & 0 & -\kappa^1 u^1 \\ 0 & \lambda^2 & 0 & 0 & -\kappa^2 u^2 \\ 0 & 0 & \lambda^3 & 0 & -\kappa^3 u^3 \\ 0 & 0 & 0 & \lambda^4 & -\kappa^4 u^4 \\ 0 & 0 & 0 & 0 & 0 \end{pmatrix} \partial_x \begin{pmatrix} u^1 \\ u^2 \\ u^3 \\ u^4 \\ a \end{pmatrix} + \begin{pmatrix} \partial_x \kappa^1 a u^1 \\ \partial_x \kappa^2 a u^2 \\ \partial_x \kappa^3 a u^3 \\ \partial_x \kappa^4 a u^4 \\ R(a,u) \end{pmatrix} = 0 \quad (4.7)$$

where λ^α denote the characteristic velocities depending on a and the κ^α are reaction rates of the form $\pm\delta\,\kappa_{B/P}$, possibly variable in space and time.

Given sufficiently smooth initial data and smooth coefficients, the Cauchy problem for this system possesses a unique smooth solution for small times but the formation of discontinuities from smooth data cannot be excluded for large times. To get a feeling how these shocks look like we solve a specific Riemann problem for this system with constant reaction parameters so that $\partial_x \kappa^\alpha \equiv 0$.

Let us consider a situation as sketched in Fig. 9 where

$$u_l^3 = p_l, \quad u_l^4 = 0 \qquad \text{and} \qquad u_r^3 = 0, \quad u_r^4 = b_r. \quad (4.8)$$

The monomer densities on the left and right of the shock in this simplest possible example should be given by a_P and a_B, leading to characteristic velocities

$$\lambda_l^3 = -v_P(a_P) = v_R \qquad \text{and} \qquad \lambda_r^4 = v_B(a_B) = -v_R \quad (4.9)$$

and ensuring that no monomers are produced or consumed outside the shock.

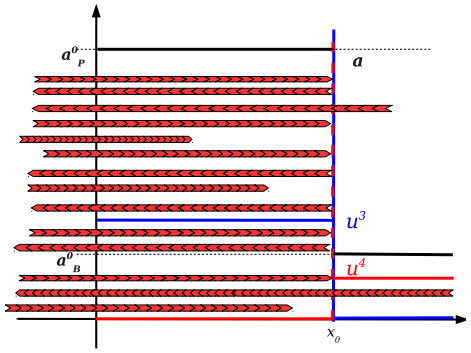

Figure 9: Cartoon of filament distributions and monomer density for the examplary shock solution with two end densities in the hyperbolic limit system. The filament ends move into the shock and accumulate there. The left tips of all filaments are assumed to be far to the left.

Inside the shock, the filament tips lead to a constant production and consumption of monomers which has to be balanced by the flux of monomers into or out of the shock by its movement. Starting with the discontinuity at $x = 0$ and denoting the shock position by $S(t)$ and its velocity by $s(t)$, we obtain

$$0 = (v_R - s)(v_R t - S)p_l - (v_R + s)(v_R t + S)b_r - (a_P - a_B)s \quad (4.10)$$

where the first two terms account for the production and consumption of monomers by filament tips, and the last term is the net flux of monomers to the shock due to its motion. Here $(v_R t - S)p_l$ and $(v_R t + S)b_r$ are the numbers of pointed and barbed ends accumulated in the shock up to time t. This translates into an equation for the shock curve,

$$0 = (dS - v_R \Sigma t)\dot{S} - (a_P - a_B)\dot{S} - v_R \Sigma S + d v_R^2 t \quad (4.11)$$

where we introduced $\Sigma := p_l + b_r$ and $d := p_l - b_r$.

For the symmetric situation $d = 0$ with initial condition $S(0) = 0$, the unique solution is a standing shock $S(t) \equiv 0$. If however $p_l > b_r$, the initial velocity of the shock is positive and remains so as time proceeds. As the δ-peaks at the shock position grow, we have

$$\dot{S}(t) \to s_\infty = \left(\frac{\Sigma}{d} - \sqrt{\frac{\Sigma^2}{d^2} - 1} \right) v_R \qquad \text{as } t \to \infty. \tag{4.12}$$

In fact, $s_\infty \searrow 0$ for $d \searrow 0$ and $s_\infty \nearrow v_R$ for $d \nearrow \Sigma$ which corresponds to $p_l \gg b_r$. The dependence of the asymptotic velocity on $\mu := b_r/p_l$ is sketched in Fig. 10.

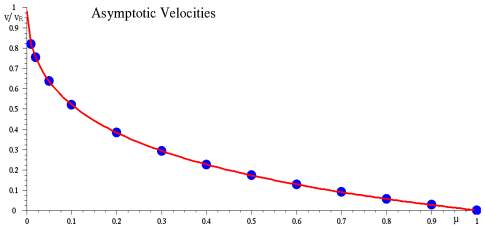

Figure 10: Asymptotic shock speed in units of v_R, depending on the ratio $\mu = u_r^4/u_l^3$. *red line*: calculated by (4.12), *blue bullets*: obtained from simulations of the ordinary differential equation (4.11).

Now we consider a more complicated situation with finite densities u^3 and u^4 on both sides of the shock. Then a_l and a_r can be different from a_P and a_B, and the conditions for them to be constant read

$$\kappa_P u_i^3 (a_P - a_i) = \kappa_B u_i^4 (a_i - a_B) \qquad \text{for } i = r, l. \tag{4.13}$$

Moreover we have to require

$$\lambda^3(a_l) u_l^3 + \lambda^3(a_r) u_r^3 > 0 \qquad \text{and} \qquad \lambda^4(a_l) u_l^4 + \lambda^4(a_r) u_r^4 > 0$$

to ensure a net gain of filament tips to the shock. Otherwise we would deal with a kind of rarefaction wave.

After some tedious calculations which can be found in [8] we obtain conditions for such shocks under our natural assumptions on the parameters. We found positive end densities $u_{l/r}^3$ and $u_{l/r}^4$ such that the Riemann problem with these data exhibits a δ-shock solution as described above whenever either

$$a_l, a_r \in (a_-, a_+) \qquad \text{or} \qquad a_l, a_r \in (a_B, a_P) \backslash [a_-, a_+] \tag{4.14}$$

where $a_\pm$ are the roots of

$$2\delta\, \kappa_P \kappa_B (a_P - a)(a - a_B) - (\kappa_B (a - a_B) + \kappa_P (a_P - a)) v_R = 0 \tag{4.15}$$

solved for a. These roots are real and satisfy $a_B < a_- < a_+ < a_P$ whenever Cond. 3.1 holds, in particular $\delta\, \kappa_P (a_P - a_B) > v_R$.

Given such monomer densities $a_{l/r}$ and having fixed one of the end densities, say u_r^3, we can also compute the other end densities from the Rankine-Hugoniot

conditions and the conditions (4.13) (for details cf. [8]):

$$u_r^4 = \frac{\kappa_P(a_P - a_r)}{\kappa_B(a_r - a_B)} u_r^3 \tag{4.16}$$

$$u_l^4 = \frac{v_R\left(1 + \frac{\kappa_P(a_P - a_r)}{\kappa_B(a_r - a_B)}\right) - 2\delta\,\kappa_P(a_P - a_r)}{v_R\left(1 + \frac{\kappa_B(a_l - a_B)}{\kappa_P(a_P - a_l)}\right) - 2\delta\,\kappa_B(a_l - a_B)} u_r^3 \tag{4.17}$$

$$u_l^3 = \frac{v_R\left(1 + \frac{\kappa_P(a_P - a_r)}{\kappa_B(a_r - a_B)}\right) - 2\delta\,\kappa_P(a_P - a_r)}{v_R\left(1 + \frac{\kappa_P(a_P - a_l)}{\kappa_B(a_l - a_B)}\right) - 2\delta\,\kappa_P(a_P - a_l)} u_r^3. \tag{4.18}$$

4.3 Numerical results involving shock like patterns

So far we showed that there exist weak solutions to the full problem consisting of isolated δ-peaks for the end densities and a continuous, piecewise smooth monomer distribution. Moreover, we found shock solutions with δ-peaks and plateaus for the end densities and discontinuous monomer concentration for the hyperbolic limit system without monomer diffusion. It remains open whether the first type of shocks can be expected to emerge from smooth data, and whether the latter type exists for $D > 0$.

These questions are difficult to tackle analytically, so we will start with simulations here. Focusing on the first type of shocks we will use initial data consisting of smooth but concentrated end densities and a smoothly varying monomer concentration as indicated in Fig. 11, left.

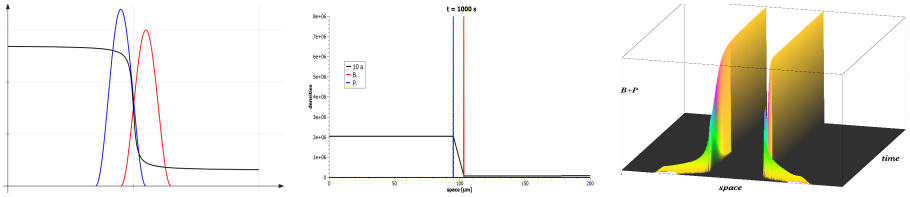

Figure 11: An example for smooth peaks of end densities as initial conditions (*left*) with different numbers of barbed and pointed ends. *red*: B_r, *blue*: P_l, *black*: a. The units of the ordinate are arbitrary. *Center*: typical steady state pattern evolving from *symmetric* initial conditions with equally many barbed as pointed ends. Notice the linearly interpolated monomer density between the peaks. *Right*: typical evolution of a standing profile emerging from a *symmetric* initial end distribution. The peaks choose their distance according to (4.4) rather than maintaining their initial distance. The (left) pointed end peak achieves its δ shape more slowly than the barbed end peak due to the slower reaction kinetics.

We observe profiles with sharp, δ-like peaks for the end densities and a continuous, piecewise smooth monomer concentration emerge from this type of initial conditions.

Depending on the relative sizes of the initial peaks of barbed and pointed ends we find either a standing profile in case of equal masses in both peaks (cf. Fig. 11) or a moving profile for different numbers of barbed and pointed ends. Both, the distance between the peaks and for moving profiles also the velocity at which the profile moves, nicely match the predicted values from the calculations

above. Moreover, the monomer profile between the peaks indeed appears to be linear in the symmetric, non-moving case and has an exponential shape in the asymmetric, moving setting.

We now discuss the more delicate shock like solutions of the second type with discontinuous monomer density. We are again interested in the emergence of shocks from smooth data. So we consider initial distributions as sketched in Fig. 12 where the plateaus of the end densities have smooth flanks.

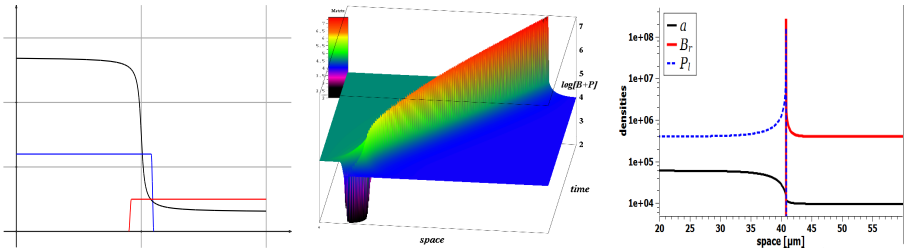

Figure 12: Simulations for shocks of the second type. *Left*: typical initial conditions with asymmetric end densities. *Center*: typical evolution of a moving shock with asymmetric end densities and constantly growing peaks (shown as $\log[B_r + P_l]$). The plateau to the left consists of pointed ends, the one to the right of barbed ends. Initially the peaks form at a finite distance from one another with a gap practically void of filament tips between them. *Right*: typical pattern evolving from symmetric plateau values $b_r = p_l$. The monomer density is smoothed by monomer diffusion. We used the logarithmic scale in the last two graphs to make both, the peaks and plateaus visible.

The resulting profiles are very similar to those predicted by the analysis of the fully hyperbolic system with $D = 0$, i.e. they soon develop very sharp Dirac peaks in the end densities. These peaks are constantly growing as filament tips are transported into them, and the positions of the barbed and the pointed end peak coincide after a brief initial phase. Moreover, for different heights of the barbed and pointed end plateaus we observe the expected moving profiles.

The finite monomer diffusion introduces though a few remarkable deviations from the predictions of the hyperbolic theory. First, the jump in the monomer distribution is not reproduced by the simulations with $D > 0$. We observe a sharp but yet smooth drop of the monomer concentration across the peak position which is already significantly non-constant in the vicinity of the shock.

By this variation in the monomer concentration the end densities are affected as well, and they exhibit smooth tails where the peaks are blended into the plateaus. Thus, the diffusion seems to blur the sharp Dirac peaks predicted for the hyperbolic system.

So the sharp accumulation of filament tips in a kind of polymerization front remains intact even for $D > 0$ with some minor changes in the precise shape of the peaks whereas the monomer gradient is kept bounded by the diffusion and gradient blow-up does apparently not occur.

5 Conclusion and discussion

We analyzed a minimal model for the polymerization dynamics of the actin cytoskeleton of a motile cell with moving boundary conditions accounting for

the motion of the cell membrane pushed by actin filament tips. Given smooth initial data and parameters we can guarantee the existence of classical smooth solutions for small times but have to expect the emergence of shocks in the long run.

The shocks we showed to exist as non-classical solutions, consist of Dirac peaks of filament tips accompanied by strong spatial variations of the monomer density. Basic versions of these peaks were seen to emerge in simulations from simple, yet smooth, initial data. More complex variants of these peaks were observed in simulations of the whole cytoskeleton model where they can be interpreted as actin polymerization fronts. We would like to emphasize that these peaks do not mean an explosion of the F-actin concentration but rather account for jump discontinuities in the filament densities.

For the fully hyperbolic system without monomer diffusion ($D = 0$) we also find solutions with discontinuous monomer concentration. Simulations indicate that these jumps are smoothed in case $D > 0$.

Finally, we ran some simulations of the full cytoskeleton model with symmetric initial conditions which indicate a resting cell in order to invesigate the polarization of the cell upon spatial variations of the reaction parameters which account for the polymerization and depolymerization of actin monomers at filament tips. In order to obtain a fast and significant displacement of F-actin we need changes in reaction dynamics at both, barbed and pointed ends.

Remarkably, the most effective variation proved to be a simultaneous change of the pointed end critical concentration a_P and the reaction rate constant κ_B at barbed ends. The former accounts for an easier dissociation of monomers from pointed ends by decreasing there binding affinity, an effect which is reported to be induced by ADF/cofilin. The enhanced reaction rate at barbed ends may be mediated by the action of formins together with sequestering actin monomers by profilin under the presence of ATP which we assumed to be available in abundance. Any other combination of only two parameters changes produced far weaker effects on the polarization of the cytoskeleton.

For the initiation of a shift of F-actin to the right and thus the emergence of a pre-lamellipodium we did not need to account for filament branching and nucleation, barbed end capping or additional control mechanisms. This is in accordance with our earlier results for the problem with fixed boundary in [7]. However, we cannot make any assertions about the relevance of these effects for the emergence of a dense actin meshwork which is necessary for the lamellipodial movement in vivo.

In the future we would like to include mechanical forces at the membrane and between the cytoskeleton and the substrate into the model in order to explain the displacement of the whole cell at later stages of motion. Further generalizations to be considered are a two dimensional formulation of the model to account for more complex movement of individual filaments and the incorporation of the filament length as a structure parameter in order to allow for nucleation and total depolymerization of filaments as done in [5].

6 Appendix - Parabolic Hölder spaces

Here we briefly discuss the notions of parabolic distance, space-time domains and parabolic Hölder spaces we used before. We will only present the case of one

space dimension but generalization to the n-dimensional case is straightforward.

Let us consider a space-time domain $Q_T \in \mathbb{R} \times \mathbb{R}^1$ given by

$$Q_T = \{(t,x) \mid 0 < t < T, l(t) < x < r(t)\} \tag{6.1}$$

where $l, r : (0,T) \to \mathbb{R}^1$ are continuous functions such that $l(t) < r(t)$ for each $t \in (0,T)$. If r and l are also continuous on $[0,T]$, the closure of Q_T is given by $\{(t,x) \mid 0 \le t \le T, l(t) \le x \le r(t)\}$. This is assumed in the following.

Definition 6.1. *1. Given (t,x), $(s,y) \in \mathbb{R} \times \mathbb{R}^1$ we define the* parabolic distance between (t,x) and (s,y) *to be*

$$|(t,x) - (s,y)|_P := \max\{|x-y|, \sqrt{|s-t|}\}. \tag{6.2}$$

2. Given $(t,x) \in \mathbb{R} \times \mathbb{R}^1$ and $r > 0$ we define the parabolic cylinder of radius r below (t,x) *by*

$$\mathrm{Cyl}_r(t,x) := \left\{(s,y) \in \mathbb{R} \times \mathbb{R}^1 \mid s < t, |(t,x) - (s,y)|_P < r\right\} \tag{6.3}$$

3. For a space-time domain Q_T given by (6.1) we define its

- parabolic boundary *to be*

$$\mathcal{P}Q_T := \left\{(t,x) \in \partial Q_T \mid \forall r > 0 : \ \mathrm{Cyl}_r(t,x) \cap \left((\mathbb{R} \times \mathbb{R}^1) \backslash Q_T\right) \neq 0\right\}$$

- top *or* open boundary *by* $\mathcal{T}Q_T := \partial Q_T \backslash \mathcal{P}Q_T$
- bottom *or* base *by*

$$\mathcal{B}Q_T := \left\{(t,x) \in \mathcal{P}Q_T \mid \mathrm{Cyl}_r(t + r^2, x) \subset Q_T \text{ for some } r > 0\right\}$$

- lateral boundary *by* $\mathcal{L}Q_T := \mathcal{P}Q_T \backslash \overline{\mathcal{B}Q_T}$
- corner points *by* $\mathcal{C}Q_T := (\mathcal{P}Q_T \cap \overline{\mathcal{B}Q_T}) \backslash \mathcal{B}Q_T$.

4. The spatial diameter *of the domain Q_T is given by*

$$\operatorname{diam} Q_T := \sup_{(t,x),(s,y) \in Q_T} \{|x-y|\} \tag{6.4}$$

5. For $t \in \mathbb{R}$ define the (closed) temporal section through Q_T at t *by*

$$\Sigma_t := \left\{x \in \mathbb{R}^1 \mid (t,x) \in \overline{Q_T}\right\}. \tag{6.5}$$

Note that $\mathcal{P}Q_T$ is that part of the boundary of Q_T through which a parabolic equation can transport information into the domain via boundary or initial conditions. More precisely, the bottom $\mathcal{B}Q_T$ is that part of the boundary where information can only enter the domain, the lateral boundary $\mathcal{L}Q_T$ is the part which can receive information from outside as well as from inside the domain, whereas to the top $\mathcal{T}Q_T$ information can only be transported from within the domain. We therefore have to provide initial conditions on $\mathcal{B}Q_T$, boundary conditions on $\mathcal{L}Q_T$ and cannot impose any conditions at $\mathcal{T}Q_T$.

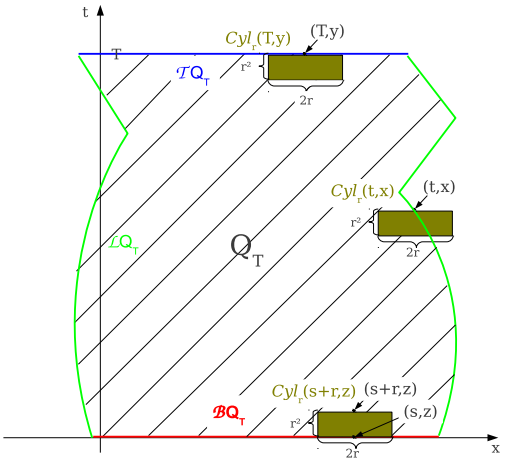

Figure 13: Sketch of a typical space-time domain Q_T with the respective parts of the boundary, and a parabolic cylinder of radius r being sketched for three boundary points. Note that beneath (T, y) there is some parabolic cylinder which has no point in common with the exterior of Q_T whereas any parabolic cylinder beneath (t, x) reaches beyond the boundary of Q_T.

Furthermore, in our particular setting, we can write these parts of the boundary in simpler terms as

$$\begin{aligned}
\mathcal{B}Q_T &= \{(0,x) \mid l(0) < x < r(0)\} \\
\mathcal{T}Q_T &= \{(T,x) \mid l(T) < x < r(T)\} \\
\mathcal{L}Q_T &= \{(t,l(t)) \mid 0 < t < T\} \cup \{(t,r(t)) \mid 0 < t < T\} \\
\mathcal{C}Q_T &= \{(0,l(0)),(0,r(0))\}.
\end{aligned}$$

With this set of notation we can now define the parabolic Hölder spaces.

Definition 6.2. *Given a space-time domain $Q_T \in \mathbb{R} \times \mathbb{R}^1$, for any function $f \in C^\infty(\overline{Q_T})$ and any numbers $k \in \mathbb{N}_0$ and $\beta \in (0,1)$ define*

$$\|f\|_{C^{k+\beta,P}} := \sum_{m+2j \le k} \|\partial_x^m \partial_t^j f\|_{C^0} + [f]_{k+\beta} + \langle f \rangle_{k+\beta} \tag{6.6}$$

where

$$\begin{aligned}
[f]_{k+\beta} &= \sum_{m+2j=k} \sup_{\substack{(t,x),(s,y) \in Q_T \\ (t,x) \neq (s,y)}} \frac{|\partial_x^m \partial_t^j f(t,x) - \partial_x^m \partial_t^j f(s,y)|}{|(t,x)-(s,y)|_P^\beta} \\
&\equiv \sum_{m+2j=k} H\ddot{o}l_{P,\beta}(\partial_x^m \partial_t^j f)
\end{aligned} \tag{6.7}$$

and

$$\begin{aligned}
\langle f \rangle_{k+\beta} &= \sum_{m+2j=k-1} \sup_{\substack{(t,x),(s,x) \in Q_T \\ s \neq t}} \frac{|\partial_x^m \partial_t^j f(t,x) - \partial_x^m \partial_t^j f(s,x)|}{|t-t_0|^{\frac{1+\beta}{2}}} \\
&\equiv \sum_{m+2j=k-1} H\ddot{o}l_{t,\frac{1+\beta}{2}}(\partial_x^m \partial_t^j f)
\end{aligned} \tag{6.8}$$

are the parabolic and the temporal Hölder constants of the highest relevant combinations of derivatives of f, respectively.

A function $f \in C^0(\overline{Q_T})$ *is called* parabolically Hölder continuous with exponent β *if* $\|f\|_{C^{0+\beta,P}} < \infty$*, and* f *is* of class $C^{k+\beta,P}$ *if* $\|f\|_{C^{k+\beta,P}} < \infty$*.*

The definitions in [13] lead to precisely the same spaces with equivalent norms. The first difference is the restriction to finite distances in the definition of the Hölder constants which does no harm if Q_T is bounded in space. The second change consists of splitting up the parabolic Hölder constant into a spatial and a temporal component, roughly corresponding to a replacement of our parabolic distance by $|x-y|+\sqrt{|s-t|}$ which is of course equivalent. This second alteration can be accounted for by a factor of 2 in the definition of the norms.

Below we give the explicite expressions of the most widely used parabolic Hölder norms for functions f defined on $\overline{Q_T}$.

$$\|f\|_{C^{0+\beta,P}} = \|f\|_{C^0} + H\ddot{o}l_{P,\beta}(f),$$
$$\|f\|_{C^{2+\beta,P}} = \|f\|_{C^{2_x,1_t}} + H\ddot{o}l_{P,\beta}(\partial_{xx}f) + H\ddot{o}l_{P,\beta}(\partial_t f) + H\ddot{o}l_{t,\frac{1+\beta}{2}}(\partial_x f).$$

Remark 6.1. *(Hölder scale) As is the case with conventional Hölder spaces, we have the compact embedding*

$$C^{k+\beta_1,P}(\overline{Q_T}) \hookrightarrow\hookrightarrow C^{l+\beta_2,P}(\overline{Q_T})$$

for integers $0 \le l \le k$ *and exponents* $0 < \beta_2 < \beta_1 \le 1$*. For the solution operators in Sec. 3 to be contractions we need the embedding constants for the case* $k = l = 0$*. It is easily seen that*

$$\begin{aligned} H\ddot{o}l_{P,\beta_1}(f) &= \sup_{\substack{(t,x),(s,y)\in Q_T \\ (t,x)\neq(s,y)}} |(t,x)-(s,y)|_P^{\beta_2-\beta_1} \frac{|f(t,x)-f(s,y)|}{|(t,x)-(s,y)|_P^{\beta_2}} \\ &\le \left(\max\left\{\operatorname{diam} Q_T, \sqrt{T}\right\}\right)^{\beta_2-\beta_1} H\ddot{o}l_{P,\beta_2}(f) \end{aligned} \tag{6.9}$$

so that the embedding constant only depends on β_1*,* β_2*, and the size of* Q_T*.*

The particular Hölder scale for functions $g : [0,T] \to \mathbb{R}$ *of one real variable is also useful as it applies to the boundary curves. For these we simply have*

$$H\ddot{o}l_{\beta_1}(g) \le T^{\beta_2-\beta_1} H\ddot{o}l_{\beta_2}(g) \tag{6.10}$$

and the embedding constant obviously tends to zero as T *does.*

Acknowledgement The work of Jan Fuhrmann was partially supported by a grant from the German Ministry of Education and Research (BmBF, 01GQ1003A).

References

[1] Armstrong M T, Armstrong P B, *Cell motility in fibroblast aggregates*, J Cell Sci **33** (1978), 37–52

[2] Bugyi B, Carlier M-F, *Control of actin filament treadmilling in cell motility*, Annu Rev Biophys **39** (2010), 449–470

[3] Coddington E A, Levinson N, *Theory of ordinary differential equations*, McGraw-Hill, Inc., New York (1995)

[4] DiPerna R J, Lions P-L, *Ordinary differential equations, transport theory and Sobolev spaces*, Invent Math **98** (1989), 511–547

[5] Doubrovinski K, Kruse K, *Self-alignment in systems of treadmilling filaments*, Eur Phys J E **31** (2010), 95–104

[6] Freistühler H, Fuhrmann J, Stevens A, *Traveling waves emerging in a diffusive moving filament system*, in Managing complexity, reducing perplexity. Modeling biological systems, Eds. Ajmone-Marsan G, Delitala M, Springer, 2013 (to appear)

[7] Fuhrmann J, Käs J, Stevens A, *Initiation of cytoskeletal asymmetry for cell polarization and movement*, J Theor Biol **249** (2007), 278–288

[8] Fuhrmann J, *On a minimal model for the initiation of cell movement*, PhD thesis, Heidelberg (2012)

[9] Goode B L, Eck M J, *Mechanism and function of formins in the control of actin assembly*, Annu Rev Biochem **76** (2007), 593–627

[10] Haastert, P J M van, *Amoeboid cells use protrusions for walking, gliding and swimming*, PLoS ONE **6** (2011): e27532

[11] Jaffe A B, Hall A, *Rho GTPases: Biochemistry and Biology*, Annu Rev Cell Dev Biol **21** (2005), 247–269

[12] Kiuchi T, Ohashi K, Kurita S, Mizuno K, *Cofilin promotes stimulus-induced lamellipodium formation by generating an abundant supply of actin monomers*, J Cell Biol **17** (2007), 465–476

[13] Ladyženskaja O A, Solonnikov V A, Ural'ceva N N, *Linear and quasilinear equations of parabolic type* (corrected reprint), Translations of Mathematical Monographs, American Mathematical Society, Providence, R.I. (1988)

[14] Lieberman G M, *Second order parabolic differential equations*, World Scientific Publishing, Singapore (1996)

[15] Okabe S, Hirokawa N, *Actin dynamics in growth cones*, J Neurosc **11**.7 (1991), 1918–1929

[16] Pantaloni D, Carlier M-F, *How profilin promotes actin filament assembly in the presence of thymosin-β_4*, Cell **75**.5 (1993), 1007–1014

[17] Plastino J, Lelidis I, Prost J, Sykes C, *The Effect of Diffusion, Depolymerization and Nucleation Promoting Factors on Actin Gel Growth*, Eur Biophys J **33** (2004), 310–320

[18] Pollard T D, *Rate constants for the reactions of ATP- and ADP-actin with the ends of actin filaments*, J Cell Biol **103** (1986), 2747–2754

[19] Ponti A , Machacek M, Gupton S L, Waterman-Storer C M, Danuser G, *Two Distinct Actin Networks Drive the Protrusion of Migrating Cells*, Science **305**.5691 (2004), 1782–1786

[20] Yamaguchi H, Condeelis J, *Regulation of the actin cytoskeleton in cancer cell migration and invasion*, Biochim Biophys Acta **1773** (2007), 642–652